ELSEVIER

Composite Structures 46 (1999) 367–379

COMPOSITE STRUCTURES

High performance 3D-analysis of thermo-mechanically loaded composite structures

R. Rolfes *, J. Noack, M. Taeschner

German Aerospace Center, Institute of Structural Mechanics, 38106 Braunschweig, Germany

Abstract

This paper considers the analysis of composite structures, simultaneously loaded by mechanical and thermal loads, as often found in aerospace applications. Typically a thermal analysis providing the temperature field must precede the stress analysis, which has to account for thermal as well as for additional mechanical loads. Presently, thermal analyses are mostly carried out by finite difference methods or by 3D finite elements, whereas the stress analysis is usually performed by the use of shell elements. Thus, the temperature field has to be transferred from a finite difference or 3D finite element model to a shell finite element model. This process often requires lots of manual user interaction and can get very time consuming. The paper suggests an integrated analysis process which uses a shell finite element model throughout. Thermal lamination theories and related finite elements developed by the first author are used for the 3D thermal analysis. This leads to a reduction of the computing time by two orders of magnitude as compared to 3D finite elements whereas the accuracy of the results is nearly unaffected. The stress analysis is carried out using the same geometry model but with different mesh density. Interpolation between the different meshes can be accomplished automatically since both discretizations are defined on the same geometry. Standard shell elements based on the First order shear deformation theory (FSDT) provide the three in-plane stress components. A novel postprocessing scheme is adopted for determining all transverse stress components from the in-plane stresses and the temperature field. The postprocessing methodology is based on the extended 2D-method which utilizes the material law for transverse shear and the 3D equilibrium conditions. It is computationally very efficient and can be applied in conjunction with any standard finite element package. The interaction of thermal and stress analysis is demonstrated by the example of a composite wing box for a future large airliner.

Keywords: Finite elements; Transverse stresses; Thermal analysis; Thermo-mechanical bahaviour; Wing box

1. Introduction

An increasing amount of modern aerospace structures is built from composite materials. Many of these structures are simultaneously loaded by high thermal and mechanical loads. Typical examples are the wings for the next generation of commercial airliners, which are exposed to high sun irradiation, large orbital structures under thermal cycling, the load carrying structure of future reusable launchers or advanced propulsion components. In all cases the stress analysis must be preceded by an accurate thermal analysis, which is to provide the temperature input data required for the stress analysis. Since most of the aerospace structures are thin-walled the stress analysis is often carried out assuming plane stress conditions and thus neglecting the stress components in transverse direction, i.e., the transverse shear stresses and the transverse normal stress. While this simplification is reasonable for homogenous isotropic structures, it can be dangerous in the case of laminated composite structures. Experimental investigations [20] have shown that failure can occur in a transverse shearing mode when certain combinations of in-plane compression and in-plane shear are acting. This failure is significantly influenced by transverse shear stresses. Furthermore, the development and progression of delaminations, which are eventually the most severe type of damage in laminated composites, is very much influenced by transverse stresses. Although the importance of transverse stresses rises with increasing wall thickness, they should not be neglected in thin-walled structures as well. Consequently, advanced failure criteria for composites [7,11,20] account for the full 3D state of stress.

Thermal analysis of composite structures must cope with the fact that many composite materials are not only

* Corresponding author.

0263-8223/99/$ - see front matter
PII: S0263-8223(99)00101-4

mechanically but also thermally anisotropic. This is expressed by the ratio of the thermal conductivities in fibre direction and perpendicular to it. Especially, for carbon fibre reinforced plastics (CFRP) a high ratio is observed ranging from about 6 to 450, depending on the type of fibre [3]. Furthermore, the principal direction of heat conduction changes from layer to layer which is why the problem becomes inhomogeneous. Surana and co-workers [4,34] have developed finite elements for axisymmetric problems with variable polynomial degree of the shape functions in longitudinal as well as in the radial direction. The functions in radial direction were defined over the whole laminate thickness in [34] whereas layerwise approximations were chosen in [4]. Both methods are predominantly suited for very thick-walled cylindrical structures. Thin-walled structures have been already calculated by Padovan [17] using a layerwise discretization with orthotropic 3D-elements. However, this is a very costly process with respect to modelling and calculation time. Tamma and Yurko [36] have reduced the effort by modelling a couple of layers with only one orthotropic 3D-element. When simply evaluating the finite element conduction matrix by a layerwise integration they could not account for the stacking sequence. This effect can be covered by the thermal lamination theories (TLT) developed by Rolfes [25–27]. They also allow for establishing 2D finite elements capable of describing the full 3D heat conduction problem. A linear temperature distribution through the thickness is assumed by the linear TLT. QUADTL, the related quadrilateral finite element, provided good results for steady-state and transient problems [25,26]. Under extremely concentrated loads and during the initial phase of transient processes, a quadratic temperature distribution is more suitable. Very good performance of the quadratic TLT and the related finite element QUADQL has been shown for linear and non-linear problems [27]. Noor and Burton [16] have proposed a predictor–corrector approach where they have applied the linear TLT in the predictor phase. For the corrector phase they have used the 3D heat conduction equation and the constitutive law in order to improve the linear temperature distribution in thickness direction. Recently, the linear TLT was used by Argyris and Tenek [1,2] in conjunction with triangular elements for solving steady-state problems with non-linearities due to the radiative boundary conditions and temperature-dependent conductivities.

Beside finite elements often finite difference methods are used for the thermal analysis of aerospace structures, whether they are metallic, hybrid or composite structures. Originally, these methods were designed for problems in which the radiation exchange between the structural parts plays the dominant role (e.g., satellites). However, the existing finite difference methods face severe problems, if the conduction of heat within the structure is important, since there is no general procedure for calculating the conduction resistors. Especially, if skewed meshes have to be used due to irregular geometry of the structures, or the material properties are anisotropic, uncertain results are yielded [6]. Furthermore, these methods require time-consuming network generations, all the more considering that an additional model is needed for calculation of radiation exchange factors. Experience of industrial partners has shown that generating a 500 node network takes about 700 h from an engineer. The authors are well aware that finite difference codes like e.g., ESATAN are widely and successfully applied by many users. They have gathered broad experience in skillful modelling which can sometimes help to overcome the problems mentioned above. Nevertheless, the application of advanced finite element methods like those described in [1,2,16,25–27] can very much contribute to enhance the thermal analysis process for composite plates and shells.

While lamination theories for the thermal analysis are relatively new, comparable developments for the stress analysis have been existing for a long time. Despite classical lamination theory (CLT) being most widely known, composite elements in general purpose FEA systems are usually based on FSDT because of their ease of implementation, since FSDT requires $C^{(0)}$-continuity for shape functions only in contrast to CLT. Comparisons by Rohwer [24] of the FSDT and several higher-order theories with analytical 3D-solutions have shown that the FSDT is a good compromise between low effort and high accuracy. While good results are achieved for the displacements and the in-plane stresses, poor values are obtained for the transverse shear stresses when calculated using the constitutive law. The main reason is the continuity of the transverse shear angles in thickness direction which results in discontinuous stresses which in turn violate the equilibrium conditions. Since all higher-order lamination theories [14,15,18,21,33] based on laminatewise approximations show this deficiency, layerwise theories with discontinuous shear angles have been suggested [5,22,32,35]. However, since the number of functional degrees of freedom increases with the number of layers, the numerical effort is in the range of a full 3D-analysis. It can be reduced by applying equilibrium conditions at the layer interfaces, but related finite elements require $C^{(1)}$-continuity of the shape functions.

If the 3D equilibrium conditions instead of the constitutive law are used, no higher-order theories are necessary for obtaining realistic transverse shear stress distributions. This procedure has already been proposed by Pryor and Barker [19]. It needs the calculation of first derivatives of the in-plane stresses with respect to the in-plane co-ordinates for determining the transverse shear stresses. If the transverse normal stress should be evaluated, one more order of differentiation is required. Pryor and Barker chose cubic shape functions in their

procedure in order to evaluate the transverse shear stresses on element level. Thus, fourth order polynomials would be required for the transverse normal stress. By choosing different functional degrees of freedom and selecting simplified shape functions for the displacements, Engblom and Ochoa [9] succeeded in lowering this requirement significantly. However, they could not fulfil the boundary conditions at both facings simultaneously. This was achieved by the extended 2D-method of Rolfes and Rohwer [28,31], which is based on two simplifying assumptions. It allows to evaluate accurately all transverse stress components in elements with only quadratic shape functions. The method has been recently extended to thermal loads [29].

The outline of the paper is as follows. First, standard analysis approaches for thermal and subsequent mechanical analysis of composite structures are demonstrated by the example of two benchmark structures. Finite elements as well as finite differences are regarded for the thermal analysis. Second, the main features of the TLT and the extended 2D-method are shown. The drastic increase of the efficiency as compared to the standard analysis approaches is demonstrated and the limitations of the procedures are discussed. Finally, the interaction of both methods is demonstrated by the example of a thermo-mechanically loaded composite wing box which is supposed to constitute the outer wing of a future large passenger aircraft.

2. Current analysis process

The current analysis process is demonstrated by the example of two benchmark problems which were developed for the European Space Agency as part of the Future European Space Transportation Investigation Program (FESTIP, [30]). Although both structures are not pure composite structures but hybrid constructions, the principal shortcomings of the analysis process are comparable to those of composite structures. The first structure is a technology demonstrator nozzle which has been investigated within the German Hypersonic Technology Program [12,13]. While the original design was a stiffened metallic structure, an alternative sandwich construction was regarded here. The sandwich consisted of a metallic honeycomb core and two facing layers at each side separated by an insulation. The facing sheets were from titanium except for the outer sheet at the hot side which was a ceramic composite (C/C). A stringer stiffened CFRP panel with multiwall metallic thermal protection system (TPS) [10] was selected for the second benchmark. Both structures are depicted in Fig. 1.

The inner surfaces of the nozzle are exposed to high heat flow rates and pressures both varying along the axis. Thus, a thermal and a mechanical analysis of the structure were necessary. The thermal analysis was carried out using finite elements. Since the thermo-physical properties of the layers are different, a layerwise discretization with 3D-elements was inevitable (conf. Fig. 2). Generating 3D-models is generally costly. Rolfes et al. [30] have studied small structural components and could show that the modelling time is about three times higher as compared to shell models. Furthermore, the computing time was extremely high, especially since non-linearities due to temperature-dependent properties and radiation exchange had to be accounted for. For the stress analysis a simple shell model turned out to be sufficient (conf. Fig. 2). However, the temperature results from the thermal model were to be transferred to this model. This process comprised a lot of handwork since there is no tool for an automatic transference at the time being.

Finite differences instead of finite elements were used for the thermal analysis of the second benchmark, whereas again finite elements were selected for the stress analysis. The thermal load was a time and space-dependent temperature prescribed on top of the TPS, the mechanical load consisted of a spatially constant dynamic pressure varying with time. Fig. 3 shows the isothermal cells of the finite difference network and the finite element shell model for the stress analysis. Again, the required models are totally different and the interpolation of the temperatures from the isothermal cells to the finite element nodes was a very lengthy work. Pure composite structures are of course a little easier to handle. However, the principle problem is the same that there is no finite shell element for heat transfer in composites and hybrid structures.

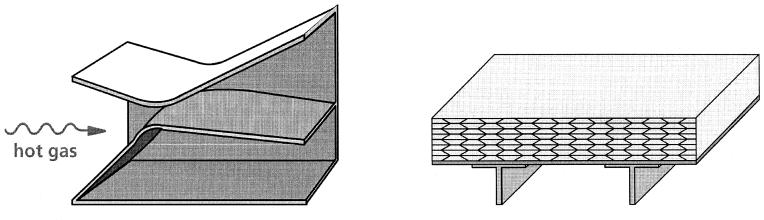

Fig. 1. Benchmark structures.

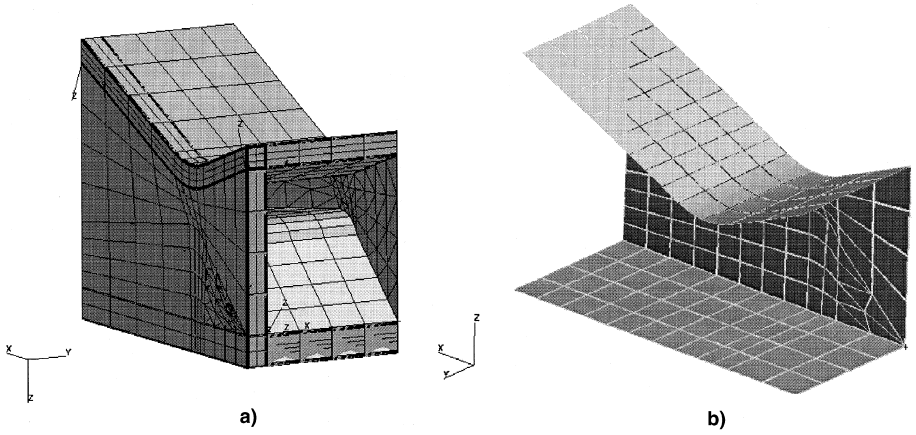

Fig. 2. Finite element meshes for the sandwich nozzle structure: (a) 3D thermal model; (b) 2D thermo-mechanical model.

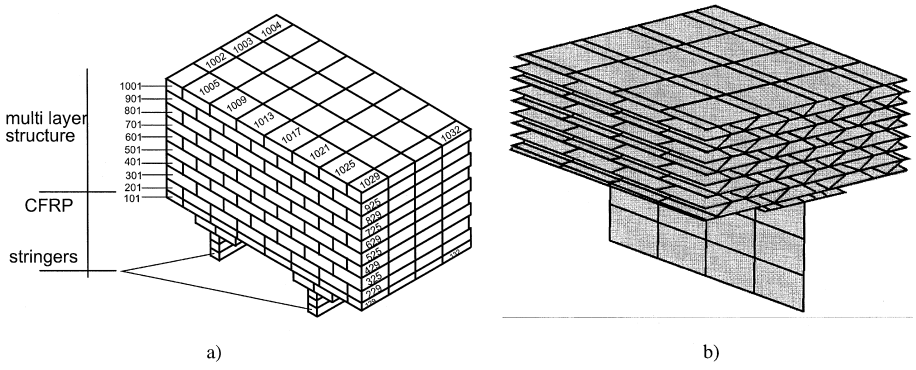

Fig. 3. Calculation models for the TPS-structure: (a) FD thermal model; (b) 2D thermo-mechanical model ([30]).

3. High performance analysis process

3.1. 3D heat transfer in composite plates

Under the prerequisites that

- the thermal conductivity in thickness direction of all layers is identical, and
- there is no heat transfer resistance at the interfaces,

the temperature distribution in thickness direction of a laminated composite plate can be expressed in many cases by a linear function. This is the fundamental assumption of the linear TLT. It can be formulated as

$$T(x_1,x_2,x_3) = T^{(0)}(x_1,x_2) + T^{(1)}(x_1,x_2)\cdot x_3, \tag{1}$$

where $T^{(0)}$ and $T^{(1)}$ are the temperature and the gradient in thickness direction of the reference plan, respectively. x_1 and x_2 are the in-plane co-ordinates while x_3 denotes the thickness coordinate. Eq. (1) can be expressed in matrix form as

$$T = \underline{X}_{\mathrm{TL}}\underline{\rho}_{\mathrm{TL}}, \tag{2}$$

where

$$\underline{X}_{\mathrm{TL}} = [\,1 \quad 0 \quad 0 \quad x_3 \quad 0 \quad 0\,] \tag{3}$$

comprises the approximation function in thickness direction and

$$\underline{\rho}_{\mathrm{TL}} = \left\{ T^{(0)} \quad T^{(0)}_{,1} \quad T^{(0)}_{,2} \quad T^{(1)} \quad T^{(1)}_{,1} \quad T^{(1)}_{,2} \right\} \tag{4}$$

is the vector of functional degrees of freedom, where a comma denotes partial differentiation w.r.t. the membrane co-ordinate. Introducing indices "TL" and "QL" for linear resp. quadratic TLT, the gradient can be written as

$$\operatorname{grad} T = \underline{Y}_{\mathrm{TL}}\,\underline{\rho}_{\mathrm{TL}} \tag{5}$$

with

$$\underline{Y}_{\mathrm{TL}} = \begin{bmatrix} 0 & 1 & 0 & 0 & x_3 & 0 \\ 0 & 0 & 1 & 0 & 0 & x_3 \\ 0 & 0 & 0 & 1 & 0 & 0 \end{bmatrix}. \tag{6}$$

This approach can be introduced into Fourier's law of heat conduction

$$q = -\tilde{\underline{K}}\cdot \operatorname{grad} T, \tag{7}$$

yielding

$$\underline{q} = -\tilde{\underline{K}}\;\underline{Y}_{\mathrm{TL}}\,\underline{\rho}_{\mathrm{TL}}. \tag{8}$$

$\underline{q}$ denotes the heat flux vector and $\underline{\tilde{K}}$ is the rank-2-tensor of the thermal conductivities of a unidirectional lamina with monoclinic symmetry. Multiplying Eq. (8) from the left-hand side by $\underline{Y}_{\mathrm{TL}}^{T}$ and integrating over the thickness provides the linear law of heat conduction of the laminate

$$\underline{\hat{Q}}_{\mathrm{TL}} = -\underline{\hat{K}}_{\mathrm{TL}}\,\underline{\rho}_{\mathrm{TL}}, \tag{9}$$

where

$$\underline{\hat{K}}_{\mathrm{TL}} = \int_h \underline{Y}_{\mathrm{TL}}^{T}\ \underline{\tilde{K}}\ \underline{Y}_{\mathrm{TL}}\ \mathrm{d}x_3 \tag{10}$$

is the linear matrix of heat conduction of the laminate and

$$\underline{\hat{Q}}_{\mathrm{TL}} = \int_h \begin{bmatrix} 0 \\ q_1 \\ q_2 \\ q_3 \\ q_1 \cdot x_3 \\ q_2 \cdot x_3 \end{bmatrix} \mathrm{d}x_3 = \begin{bmatrix} 0 \\ \hat{Q}_1 \\ \hat{Q}_2 \\ \hat{Q}_3 \\ \hat{M}_1^{(q)} \\ \hat{M}_2^{(q)} \end{bmatrix} \tag{11}$$

comprises the equivalent thermal forces. We denote $\underline{\hat{Q}}_i$ as heat flux resultants and $\underline{\hat{M}}_i^{(q)}$ as first order heat flux moments. Writing Eq. (9) in component form gives

$$\begin{bmatrix} 0 \\ \hat{Q}_1 \\ \hat{Q}_2 \\ \hat{Q}_3 \\ \hat{M}_1^{(q)} \\ \hat{M}_2^{(q)} \end{bmatrix} = - \begin{bmatrix} 0 & 0 & 0 & 0 & 0 & 0 \\ & A_{11}^{(q)} & A_{12}^{(q)} & 0 & B_{11}^{(q)} & B_{12}^{(q)} \\ & & A_{22}^{(q)} & 0 & B_{12}^{(q)} & B_{22}^{(q)} \\ & & & A_{33}^{(q)} & 0 & 0 \\ & \text{sym.} & & & D_{11}^{(q)} & D_{12}^{(q)} \\ & & & & & D_{22}^{(q)} \end{bmatrix} \begin{bmatrix} T^{(0)} \\ T_{,1}^{(0)} \\ T_{,2}^{(0)} \\ T^{(1)} \\ T_{,1}^{(1)} \\ T_{,2}^{(1)} \end{bmatrix} \tag{12}$$

with the coefficients

$$A_{ij}^{(q)} = \sum_{k=1}^{n} k_{ij}^{(k)}\ h_k, \tag{13}$$

$$B_{ij}^{(q)} = \frac{1}{2}\sum_{k=1}^{n} k_{ij}^{(k)} \left(\left(x_3^{(k+1)}\right)^2 - \left(x_3^{(k)}\right)^2 \right), \tag{14}$$

$$D_{ij}^{(q)} = \frac{1}{3}\sum_{k=1}^{n} k_{ij}^{(k)} \left(\left(x_3^{(k+1)}\right)^3 - \left(x_3^{(k)}\right)^3 \right). \tag{15}$$

Eq. (12) is very similar to the elasticity law of the laminate resulting from the CLT or FSDT. The coefficients $B_{ij}^{(q)}$ are coupling terms vanishing in case of symmetric laminates. $A_{12}^{(q)}$ and $D_{12}^{(q)}$ can be compared to the extension-shear-coupling and the bending-torsion-coupling, respectively. They are 0 for all cross-ply laminates and antisymmetric laminates with arbitrary fibre angles. It is worthwhile to notice that the heat flux resultant $\hat{Q}_3$ is always decoupled from the in-plane co-ordinates x_1 and x_2, which is due to the monoclinic symmetry of the individual layers. However, the theory can also account for non-monoclinic laminates, e.g., with fibres that are not parallel to the middle surface of the layers (stitched multi-axial laminates). There are merely additional coupling terms $A_{13}^{(q)}$, $A_{23}^{(q)}$, $B_{13}^{(q)}$ and $B_{23}^{(q)}$ to be accounted for.

Non-linear temperature distributions in thickness direction can occur in case of:

- large temperature gradients in thickness direction in conjunction with temperature-dependent thermophysical properties,
- transient problems with rapid heating, and
- spatially concentrated thermal loads.

The quadratic TLT was developed for such problems. Assuming the temperature distribution

$$T(x_1,x_2,x_3) = T^{(0)}(x_1,x_2) + T^{(1)}(x_1,x_2)\cdot x_3 + \frac{1}{2}\cdot T^{(2)}(x_1,x_2)\cdot x_3^2, \tag{16}$$

where $T^{(2)}$ is a higher-order functional degree of freedom, and then following the same line as shown for the linear TLT provides the quadratic law of heat conduction:

$$\begin{bmatrix} 0 \\ \hat{Q}_1 \\ \hat{Q}_2 \\ \hat{Q}_3 \\ \hat{M}_1^{(q)} \\ \hat{M}_2^{(q)} \\ \hat{M}_3^{(q)} \\ {}^2\hat{M}_1^{(q)} \\ {}^2\hat{M}_2^{(q)} \end{bmatrix} = - \begin{bmatrix} 0 & 0 & 0 & 0 & 0 & 0 & 0 & 0 & 0 \\ & A_{11}^{(q)} & A_{12}^{(q)} & 0 & B_{11}^{(q)} & B_{12}^{(q)} & 0 & \frac{1}{2}D_{11}^{(q)} & \frac{1}{2}D_{12}^{(q)} \\ & & A_{22}^{(q)} & 0 & B_{12}^{(q)} & B_{22}^{(q)} & 0 & \frac{1}{2}D_{12}^{(q)} & \frac{1}{2}D_{22}^{(q)} \\ & & & A_{33}^{(q)} & 0 & 0 & B_{33}^{(q)} & 0 & 0 \\ & & & & D_{11}^{(q)} & D_{12}^{(q)} & 0 & \frac{1}{2}E_{11}^{(q)} & \frac{1}{2}E_{12}^{(q)} \\ & & & & & D_{22}^{(q)} & 0 & \frac{1}{2}E_{12}^{(q)} & \frac{1}{2}E_{22}^{(q)} \\ & & & & & & D_{33}^{(q)} & 0 & 0 \\ & \text{sym.} & & & & & & \frac{1}{4}F_{11}^{(q)} & \frac{1}{4}F_{12}^{(q)} \\ & & & & & & & & \frac{1}{4}F_{22}^{(q)} \end{bmatrix} \begin{bmatrix} T^{(0)} \\ T_{,1}^{(0)} \\ T_{,2}^{(0)} \\ T^{(1)} \\ T_{,1}^{(1)} \\ T_{,2}^{(1)} \\ T^{(2)} \\ T_{,1}^{(2)} \\ T_{,2}^{(2)} \end{bmatrix}. \tag{17}$$

The second order heat flux moments are defined by

$${}^2M_i^{(q)} = \frac{1}{2}\int_h q_i x_3^2\,\mathrm{d}x_3 \tag{18}$$

and the additional coefficients of the heat conduction matrix read

$$E_{ij}^{(q)} = \frac{1}{4}\sum_{k=1}^{n} k_{ij}^{(k)}\left(\left(x_3^{(k+1)}\right)^4 - \left(x_3^{(k)}\right)^4\right),$$
$$F_{ij}^{(q)} = \frac{1}{5}\sum_{k=1}^{n} k_{ij}^{(k)}\left(\left(x_3^{(k+1)}\right)^5 - \left(x_3^{(k)}\right)^5\right). \tag{19}$$

Both theories can be favourably used for constructing special finite elements. Starting up with the weak form of the general heat conduction equation yields

$$\int_\Omega \operatorname{div}\left(\underline{\tilde{K}}\operatorname{grad} T\right) v\,\mathrm{d}\omega = \int_\Omega \rho c\dot{T} v\,\mathrm{d}\omega, \tag{20}$$

where ρ and c denote density and specific heat capacity of the composite material, ω is the domain in $\mathbb{R}^3$, and v stands for the test functions. Boundary conditions are specified as

$$T = \overline{T} \text{ on } \Gamma_1 \tag{21}$$

and

$$\underline{q}^T\underline{n} - q_c - \overline{q} = 0 \quad \text{on } \Gamma_2. \tag{22}$$

$\bar{T}$ and $\bar{q}$ are the prescribed temperature and heat flux, respectively, $\underline{n}$ is the outward normal vector at the boundary Γ_2, and q_c describes convective heat exchange by

$$q_c = h_c(T - T_{ak}). \tag{23}$$

h_c denotes the convection coefficient and T_{ak} is the ambient temperature. Thus, *Dirichlet* boundary conditions are specified on Γ_1, whereas Γ_2 comprises *Neumann* and *Robin* conditions. Eq. (22) does not take into account radiation boundary conditions. They will be added after having derived the finite element equation system. Applying Green's law to Eq. (20) allows for shifting one order of differentiation from the unknown variable T to the test functions

$$-\int_\Omega (\operatorname{grad} v)^{\mathrm{T}}\underline{\tilde{K}}\operatorname{grad} T\,\mathrm{d}\omega + \int_{\Gamma_2}\left(\underline{\tilde{K}}\operatorname{grad} T\right)^{\mathrm{T}}\underline{n} v\,\mathrm{d}\gamma = \int_\Omega \rho c\dot{T} v\,\mathrm{d}\omega. \tag{24}$$

In order to evaluate the integrals in Eq. (24) T and v and its first derivatives must be quadratic integrable functions in the Lebesgue sense. This is expressed by

$$v \in H^1(\Omega), \quad T \in H^1(\Omega). \tag{25}$$

Introducing Eqs. (2) and (5) and splitting the domain according to

$$\mathrm{d}\omega = \mathrm{d}a \cdot \mathrm{d}x_3 \tag{26}$$

yields

$$\int_A \underline{\chi}^{\mathrm{T}}\underline{\hat{K}}\underline{\rho}\,\mathrm{d}a + \int_{\Gamma_2} h_c\underline{\chi}^{\mathrm{T}}\underline{X}^{\mathrm{T}}\underline{X}\underline{\rho}\,\mathrm{d}s + \int_A \underline{\chi}^{\mathrm{T}}\underline{\hat{C}}\underline{\dot{\rho}}\,\mathrm{d}a = \int_{\Gamma_2}(h_c T_{ak} - \overline{q})\underline{\chi}^{\mathrm{T}}\underline{X}^{\mathrm{T}}\,\mathrm{d}s, \tag{27}$$

where $\underline{\chi}$ comprises the functional degrees of freedom of the test functions and $\underline{\hat{C}}$ is the heat capacity matrix of the laminate

$$\underline{\hat{C}} = \rho c\int_h \underline{X}^{\mathrm{T}}\underline{X}\,\mathrm{d}x_3. \tag{28}$$

Prescribed temperature at the top or bottom surfaces can be enforced by a Robin boundary condition with high convection coefficient h_c. The location is specified by $x_3 = \pm t/2$ in Eqs. (2) and (27). The index "TL" or "QL" is skipped from now on indicating that either of the TLTs can be applied. Finite elements are constructed by introducing approximation spaces of finite dimension. If they are chosen to be subspaces of the original spaces (conf. Eq. 25) a conform approximation is achieved, the convergence of which can be mathematically proven. Thus, it is chosen

$$T_h \in V_h, \quad v_h \in V_h \text{ with } V_h \subset H^1(\Omega). \tag{29}$$

The above conditions are fulfilled by functions in $C^{(0)}(\Omega)$. Therefore, a simple discretization using quadrilateral elements and bilinear shape functions leads to a conform finite element approximation. It is expressed by

$$\underline{\rho} = \underline{\overline{\overline{N}}}\,\underline{\vartheta}, \tag{30}$$

where $\underline{\overline{\overline{N}}}$ comprises the shape functions and $\underline{\vartheta}$ is the vector of nodal degrees of freedom. It comprises eight components for the linear TLT and 12 for the quadratic theory. The related finite elements, denoted by QUADTL and QUADQL, are depicted in Fig. 4.

Inserting Eq. (30) into Eq. (27) finally leads to the finite element equation system

$$\underline{K}\underline{\Theta} + \underline{C}\underline{\dot{\Theta}} = \underline{Q}, \tag{31}$$

where Θ is the global vector of unknowns, $\underline{Q}$ is the finite element thermal load vector, and $\underline{K}$ and $\underline{C}$ denote the finite element conduction and capacity matrix, respectively. Radiation exchange can be taken into account by adding the radiation load vector

$$\underline{Q}_s = \underline{S}\Theta^4 \tag{32}$$

to the right-hand side of Eq. (31), where $\underline{S}$ is the radiation exchange matrix (conf. [8]). However, this causes a

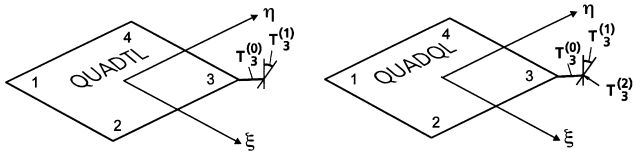

Fig. 4. Finite elements QUADTL and QUADQL.

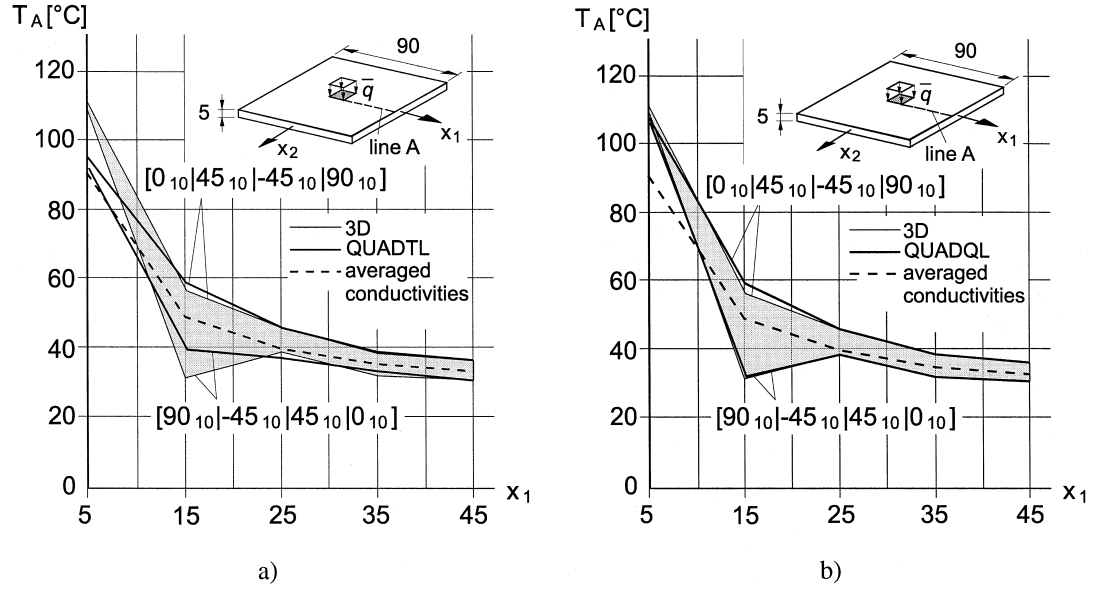

Fig. 5. Temperature distributions on top of a composite plate subjected to a concentrated heat flux for two stacking sequences (linear calculation): (a) Finite element QUADTL; (b) finite element QUADQL.

very strong non-linearity. Radiation boundary conditions can play a dominant role in high temperature applications of ceramic composites. Additional non-linearities can occur due to temperature dependence of the thermo-physical properties.

The performance of the elements QUADTL and QUADQL is demonstrated by comparing with layerwise discretizations using one HEXA-element of MSC/NASTRAN per layer (results denoted by 3D). A 40-layered plate with conductivities $k_1 = 30$ W/m K (in fibre direction) and $k_2 = 1.1$ W/m K (perpendicular to the fibre) under a concentrated heat flux of $q = 100$ kW/m^2 was calculated. There were adiabatic boundary conditions on top of the plate, whereas convection with $h_c = 30$ W/m^2 K and $T_{ak} = 0$°C was applied along the edges and at the bottom surface. Fig. 5 shows the results of a linear calculation. Both QUADTL and QUADQL are capable of reflecting the influence of the stacking sequence. When not using a TLT but instead a plate element with linear temperature distribution in thickness direction and averaged conductivities, the results cannot account for the stacking sequence. Furthermore, it can be observed that QUADTL deviates from the 3D-solution directly under the concentrated load, whereas QUADQL is very accurate throughout. The computing time for QUADQL and QUADTL was about two orders of magnitude lower as compared to the 3D-solution.

Non-linear transient calculations with temperature-dependent properties shown in Table 1 were carried out for a skin-stringer-component. The boundary conditions were the same as before. Fig. 6 shows the initial transient response at the centre of the top surface for two loading cases. Under uniform loading both elements behave favourably, under concentrated load QUADQL is significantly better. The steady-state temperature distributions (conf. Fig. 7) are nearly identical for all three calculations.

3.2. 3D stress analysis of composite plates

When a plate is subjected to changes in temperature, the distribution of which can be calculated by the methods described before, thermal strains are generated if the thermal expansion coefficient is unequal to zero. Thermally induced stresses do only appear if the free deformation of the structure is restricted by internal

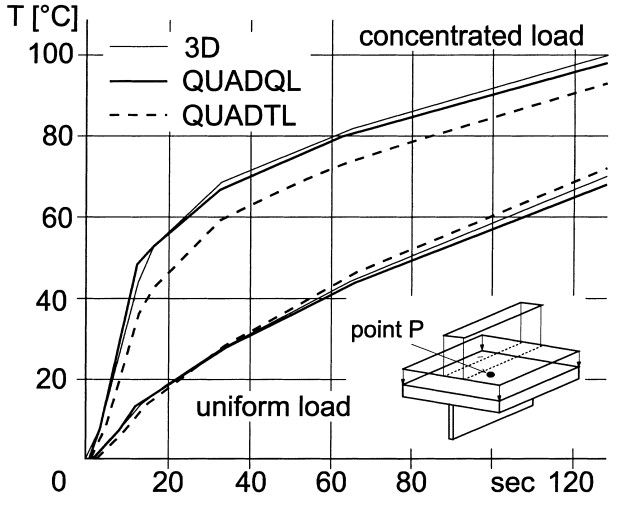

Fig. 6. Transient temperature response on top of a skin-stringer-component for two loading cases (non-linear calculation); comparison of QUADTL- and QUADQL-results.

Table 1
Properties and loading of the wing box

Lay-up			Mechanical properties
Section	Thickness (mm)	Stacking sequence	
Top surface	20.00	$[(-45_3, 0_2, +45_3, 90, 0)_{10}]_S$	$E_L = 115\,000$ N/mm^2
Bottom surface	15.00	$[(-45_4, 0_2, +45_4, 90, 0)_5]_S$	$E_L = 7750$ N/mm^2
Spars	15.00	$[(-45_4, 0_2, +45_4, 90, 0)_5]_S$	$G_{LT} = 4000$ N/mm^2
Ribs	6.00	$[(-45, +45, (-45_4, 0, 90, +45_4, 0)_2]_S$	$G_{TT} = 3200$ N/mm^2
Stringers	13.00	$[(-45, 0_5, +45, 90, 0_5)_4]_S$	$\nu_{LT} = 0.3$, $\alpha_L = 3.533 \times 10^{-7}$ 1/K
			$\alpha_T = 3.513 \times 10^{-5}$ 1/K

Thermal boundary conditions	Thermo-physical properties of M50/epoxy				Mechanical loads
	T (°C)	k_1 (W/m K)	K_2 (W/m K)	c (J/g K)	
$h_{c2}(t) = 22.815 \cdot t + 31.5$ W/m^2 K	30	54.0	0.96	0.84	$P_T = 0.004232$ (N/mm^2)
$h_{c1} = 14.2$ W/m^2 K	120	86.4	1.06	1.09	$P_B = -0.00211$ (N/mm^2)
$T_{ak} = 55^\circ$ C, $T_i = 95^\circ$ C					$M_{yt} = -477800$ (N), $M_{yb} = -238900$ (N)

constraints or boundary conditions. In-plane stresses can occur as well as transverse stresses.

In case of a uniform thermal load within the $x_1 - x_2$-plane transverse stresses can only develop near the boundaries. At free edges the transverse shear resultant must vanish, however, interlaminar shear eigen-stresses are normally present since the thermal expansion behaviour changes from layer to layer. Transverse shear resultants can develop at supported boundaries if the thermal load causes bending of the plate. This occurs in symmetric laminates under unsymmetric temperature distribution in thickness direction, or in unsymmetric laminates even under uniform through-the-thickness temperature. Thermally induced transverse stresses can occur throughout the whole plate if the thermal loading is non-uniform within the $x_1 - x_2$-plane.

Within the present paper transverse stresses due to thermal as well as mechanical loads are discussed. In-plane stresses have been broadly treated in the literature. Rohwer [24] has compared different theories and revealed that the FSDT is a good compromise between high accuracy and low computational effort. Subsequently, the extended 2D-method is presented which allows for determining all transverse stress components by a postprocessing procedure based on the FSDT. It is easily applicable in practical calculation processes, since elements relying on the FSDT are implemented into virtually any standard FE-code, and the transverse stresses can be evaluated by an independent postprocessing code.

First, some fundamental equations of the FSDT are recapitulated which are needed in the following. In-plane stress components $(\sigma_{11}, \sigma_{22}, \tau_{12})$ are calculated by

$$\underline{\sigma}_m = \underline{\tilde{C}}\left(\underline{\varepsilon}^0 + x_3\underline{\kappa} - \underline{\alpha}\,\Delta T\right), \tag{33}$$

where $\underline{\varepsilon}^0$, $\underline{\kappa}$ and $\underline{\alpha}$ are extensional strains and curvatures of the middle surface and coefficients of thermal expansion, respectively. $\underline{\tilde{C}}$ is the reduced (plane-stress) stiffness matrix, which is derived from the 3D material law for transversely isotropic material by assuming that

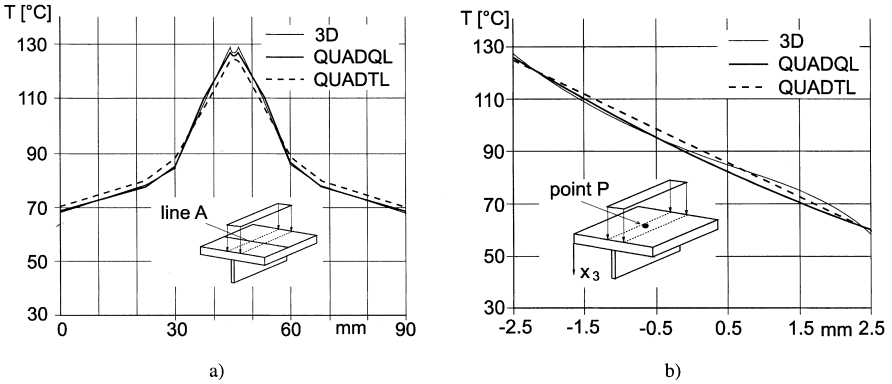

Fig. 7. Temperature distributions for a skin-stringer-component; comparison of QUADTL- and QUADQL-results (non-linear calculation): (a) temperature distribution along line A; (b) through-the-thickness temperature distribution at point P.

the transverse normal stress vanishes. Nevertheless, this stress component can be evaluated a posteriori. The transverse shear stresses if calculated from the material law read

$$\underline{\tau} = \underline{\tilde{G}}\,\underline{\gamma}, \tag{34}$$

where $\underline{\gamma}$ denotes the transverse shear angles and $\underline{\tilde{G}}$ comprises the shear moduli.

The extended 2D-method is based on five sets of equations:

1. Thermoelastic constitutive relation for the laminate

Using Eq. (33) the extensional and bending resultants are obtained by integrating over the thickness. It follows that

$$\begin{bmatrix} \underline{N} \\ \underline{M} \end{bmatrix} = \begin{bmatrix} \underline{A} & \underline{B} \\ \underline{B} & \underline{D} \end{bmatrix} \begin{bmatrix} \underline{\varepsilon}^0 \\ \underline{\kappa} \end{bmatrix} - \begin{bmatrix} \underline{N}^{\mathrm{th}} \\ \underline{M}^{\mathrm{th}} \end{bmatrix} \tag{35}$$

with

$$\begin{bmatrix} \underline{N}^{\mathrm{th}} \\ \underline{M}^{\mathrm{th}} \end{bmatrix} = \int_h \begin{bmatrix} \underline{\tilde{C}}\,\underline{\alpha}\Delta T \\ \underline{\tilde{C}}\,\underline{\alpha} x_3 \Delta T \end{bmatrix} \mathrm{d}x_3. \tag{36}$$

Solving Eq. (25) for $\underline{\varepsilon}^0$ and $\underline{\kappa}$ gives

$$\begin{bmatrix} \underline{\varepsilon}^0 \\ \underline{\kappa} \end{bmatrix} = \begin{bmatrix} \underline{\tilde{A}} & \underline{\tilde{B}} \\ \underline{\tilde{B}} & \underline{\tilde{D}} \end{bmatrix} \begin{bmatrix} \underline{N} + \underline{N}^{\mathrm{th}} \\ c + \underline{M}^{\mathrm{th}} \end{bmatrix}. \tag{37}$$

$\underline{A}$, $\underline{D}$ and $\underline{B}$ are the extensional, bending and bending–extensional coupling stiffness matrices of the laminate, respectively. $\underline{\tilde{A}}$, $\underline{\tilde{D}}$ and $\underline{\tilde{B}}$ are the respective compliance matrices.

2. Material law for transverse shear

Integrating Eq. (34) over the thickness yields the transverse shear forces

$$\underline{R} = \underline{H}\,\underline{\gamma}, \tag{38}$$

where $\underline{H}$ denotes the transverse shear stiffnesses.

3. 3D equilibrium equations

$$\sigma_{13,3} + \sigma_{11,1} + \sigma_{12,2} = 0, \tag{39}$$

$$\sigma_{23,3} + \sigma_{22,2} + \sigma_{12,1} = 0, \tag{40}$$

$$\sigma_{13,1} + \sigma_{23,2} + \sigma_{33,3} = 0. \tag{41}$$

4. Simplifying assumptions

Going back to Rohwer [23] it is assumed that the influence of $\underline{N}$ on the transverse stresses is negligible and the deformation behaviour can be approximated by two cylindrical bending modes. Thus, the following derivatives vanish:

$$\underline{N}_{,\alpha} = 0, \tag{42}$$

$$M_{11,2} = M_{22,1} = M_{12,1} = M_{12,2} = 0. \tag{43}$$

5. Equilibrium conditions for the laminate after introduction of simplifying assumptions

$$M_{11,1} = R_1, \tag{44}$$

$$M_{22,2} = R_2. \tag{45}$$

Thus saving one order of derivation which significantly lowers requirements on shape functions. Transverse stresses are obtained by the following sequence of calculation steps. Eqs. (39) and (40) are resolved with respect to σ_{13} and σ_{23} and the in-plane-stresses are replaced by the strains and curvatures using Eq. (33). They are in turn substituted by the stress resultants via Eq. (37). By introducing the simplifying assumptions all derivatives of the stress resultants can be expressed by the transverse shear forces which are to be evaluated using Eq. (38). Improved transverse shear stiffnesses [23] should be applied. The final equation for the transverse shear stresses reads

$$\underline{\tau} = \underline{f}\,\underline{R} + \underline{B}_\alpha \left(\begin{bmatrix} \underline{G} & \underline{F} \end{bmatrix} \begin{bmatrix} \underline{A}^{\mathrm{th}} & \underline{B}^{\mathrm{th}} \\ \underline{B}^{\mathrm{th}} & \underline{D}^{\mathrm{th}} \end{bmatrix} + \begin{bmatrix} \underline{a}^{\mathrm{th}} & \underline{b}^{\mathrm{th}} \end{bmatrix} \right) \begin{bmatrix} T^{(0)}_{,\alpha} \\ T^{(1)}_{,\alpha} \end{bmatrix}. \tag{46}$$

Although a matrix formulation is adopted, the Einstein summation convention is applied, and the range of Greek subscripts is 1,2. $\underline{B}_\alpha$ are the Boolean matrices

$$\underline{B}_1 = \begin{bmatrix} 1 & 0 & 0 \\ 0 & 0 & 1 \end{bmatrix} \tag{47}$$

and

$$\underline{B}_2 = \begin{bmatrix} 0 & 0 & 1 \\ 0 & 1 & 0 \end{bmatrix}. \tag{48}$$

$\underline{G}$ and $\underline{F}$ are defined by

$$\underline{G} = -\underline{a}\underline{\tilde{A}} - \underline{b}\underline{\tilde{B}}, \tag{49}$$

$$\underline{F} = -\underline{a}\underline{\tilde{B}} - \underline{b}\underline{\tilde{D}}, \tag{50}$$

where $\underline{a}$ and $\underline{b}$ are partial stiffnesses

$$\begin{bmatrix} \underline{a} \\ \underline{b} \end{bmatrix} = \int_{\varsigma = x_3^{(1)}}^{x_3} \begin{bmatrix} \underline{\tilde{C}} \\ \underline{\tilde{C}} x_3 \end{bmatrix} \mathrm{d}\varsigma. \tag{51}$$

Likewise the partial thermal stiffnesses read

$$\begin{bmatrix} \underline{a}^{\mathrm{th}} \\ \underline{b}^{\mathrm{th}} \end{bmatrix} = \int_{\varsigma = x_3^{(1)}}^{x_3} \begin{bmatrix} \underline{\tilde{C}}\,\underline{\alpha} \\ \underline{\tilde{C}}\,\underline{\alpha} x_3 \end{bmatrix} \mathrm{d}\varsigma. \tag{52}$$

The full thermal stiffnesses are obtained by extending the integration over the whole thickness,

$$\begin{bmatrix} \underline{A}^{\mathrm{th}} \\ \underline{B}^{\mathrm{th}} \\ \underline{D}^{\mathrm{th}} \end{bmatrix} = \int_h \begin{bmatrix} \underline{\tilde{C}}\,\underline{\alpha} \\ \underline{\tilde{C}}\,\underline{\alpha} x_3 \\ \underline{\tilde{C}}\,\underline{\alpha} x_3^2 \end{bmatrix} \mathrm{d}x_3. \tag{53}$$

$\underline{f}$ are the components of $\underline{F}$ multiplying those derivatives of $\underline{M}$ which remain after the introduction of Eq. (43):

$$\underline{f} = \begin{bmatrix} F_{11} & F_{32} \\ F_{31} & F_{22} \end{bmatrix}. \tag{54}$$

For the temperature distribution in thickness direction the assumption of the linear TLT is made (conf. Eq. (1)).

The transverse normal stress is evaluated by solving Eq. (41) with respect to σ_{33} and introducing Eq. (46). It reads

$$\sigma_{33}(x_3) = -\underline{b}_\alpha \underline{f}^* \underline{R}_{,\alpha} + \underline{b}_\alpha \underline{B}_\beta \left(\begin{bmatrix} \underline{G}^* & \underline{F}^* \end{bmatrix} \begin{bmatrix} \underline{A}^{\mathrm{th}} & \underline{B}^{\mathrm{th}} \\ \underline{B}^{\mathrm{th}} & \underline{D}^{\mathrm{th}} \end{bmatrix} + \begin{bmatrix} \underline{a}^{*\mathrm{th}} & \underline{b}^{*\mathrm{th}} \end{bmatrix} \right) \begin{bmatrix} T^{(0)}_{,\alpha\beta} \\ T^{(1)}_{,\alpha\beta} \end{bmatrix}, \tag{55}$$

where

$$\underline{b}_1 = [1 \quad 0], \quad \underline{b}_2 = [0 \quad 1], \tag{56}$$

and

$$\begin{bmatrix} \underline{f}^* \\ \underline{G}^* \\ \underline{F}^* \\ \underline{a}^{*\mathrm{th}} \\ \underline{b}^{*\mathrm{th}} \\ \underline{a}^* \\ \underline{b}^* \end{bmatrix} = \int_{\varsigma = x_3^{(1)}}^{x_3} \begin{bmatrix} \underline{f} \\ \underline{G} \\ \underline{F} \\ \underline{a}^{\mathrm{th}} \\ \underline{b}^{\mathrm{th}} \\ \underline{a} \\ \underline{b} \end{bmatrix} \mathrm{d}\varsigma. \tag{57}$$

Eqs. (46) and (55) might look complicated at the first glance. However, they can be evaluated very easily since the dependencies from x_1 and x_2 on the one side, and x_3 on the other side are fully decoupled. $\underline{R}$, $T^{(0)}$ and $T^{(1)}$ and its derivatives are depending on x_1 and x_2 only. They are provided by the FE thermal and stress analysis. Standard isoparametric eight-noded elements are sufficient for providing all required derivatives on element level. All other quantities are functions of x_3 only, i.e., they can be evaluated independently by a postprocessor. This code also reads the results from the FE analyses and carries out the multiplications indicated in Eqs. (46) and (55).

It is emphasized that the extended 2D-method in contrast to other equilibrium methods exactly fulfills the boundary conditions for transverse shear and transverse normal stress at both facings (top and bottom) simultaneously [29].

The performance of the extended 2D-method was checked by the example of a simply supported rectangular ($l_2/l_1 = 2$) plate with slenderness ratio $l_1/h = 5$ and stacking sequence $([0/90/0/90/0]_S$. Material properties typical for CFRP with high tenacity fibres were chosen:

$$E_1/E_2 = 15;\ G_{12}/E_2 = 0.5;\ G_{22}/E_2 = 0.3378;$$
$$v_{12} = 0.3;\ \alpha_1 = 0.139 \times 10^{-6};\ \alpha_2 = 9.0 \times 10^{-6}.$$

Two loading cases were regarded, a static transverse load p and a temperature gradient $T^{(1)}$ with $T^{(0)} = 0$.

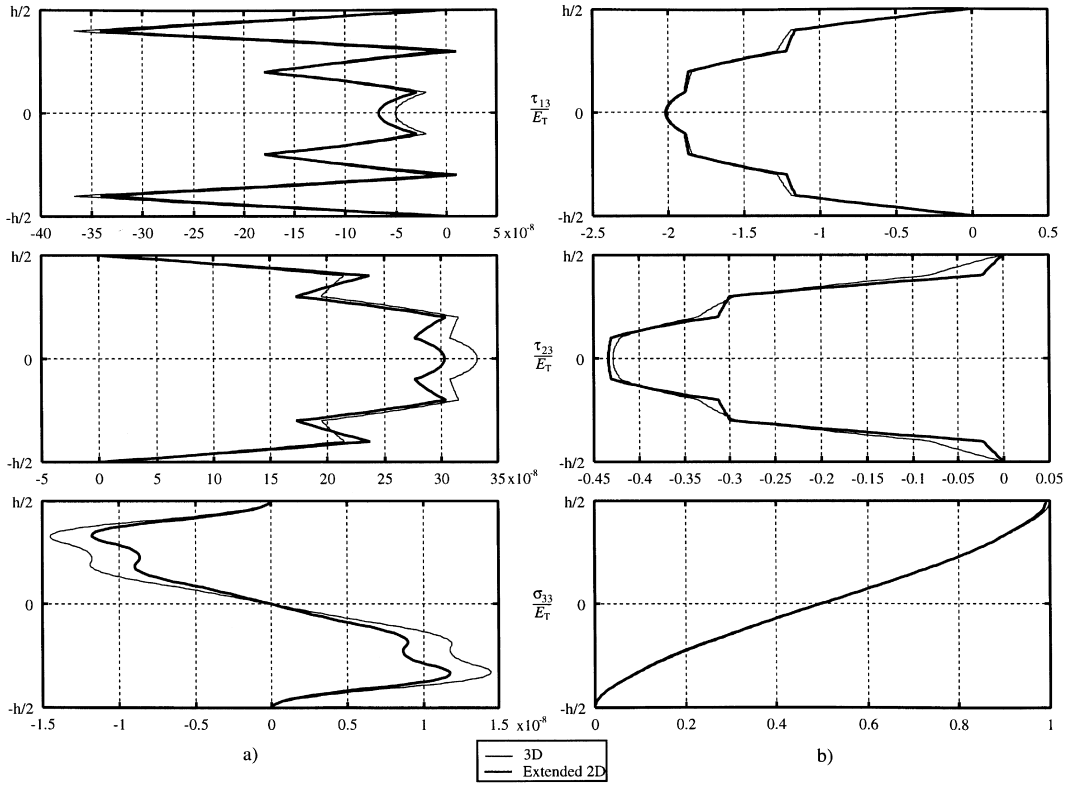

Fig. 8. Through the thickness distribution of transverse stresses in a $(0, 90, 0, 90, 0)_S$-laminate with $l_1/h = 5$ and $l_2/l_1 = 2$: (a) temperature gradient $T^{(1)}$; (b) static loading.

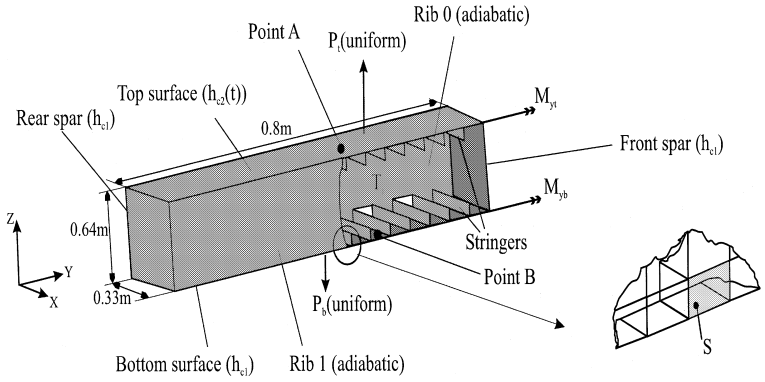

Fig. 9. Wing box with thermal boundary conditions and mechanical loads.

Both, p and $T^{(1)}$ had a double sinusoidal distribution in x_1, x_2 with an amplitude of 1 at the centre. Analytical 3D-solutions were provided by A.K. Noor. The results depicted in Fig. 8 show a very good agreement in case of static loading. Especially, the transverse normal stress is extremely accurate. The accuracy is somewhat lower in case of thermal loading. Nevertheless, the approximation is good, all the more regarding that the plate is very thick. The error decreases with increasing slenderness ratio [29]. Further numerical examples can be found in [28,31].

3.3. Combined analysis

The interaction of the high performance thermal and stress analysis is shown by the example of a composite wing box (conf. Fig. 9). All relevant data are given in Table 1.

The purpose of the investigation was to simulate the cooling process during the start of a wing that has been heated up on the ground due to high sun irradiation. Fig. 10 shows the cooling curves of the top and bottom surfaces calculated using four-noded QUADTL-elements. They are implemented into the in-house FEM-code B2000.

The stress analysis was carried out for the box fixed at upper and lower edge of rib 0 after 20 s. Eight-noded isoparametric elements were used. For simplicity the meshes were chosen in such a way that four QUADTL-elements constituted one stress element. This restriction of the mesh geometries is not necessary if standard pre- and postprocessors are used. They allow for interpolating temperature between arbitrary meshes as long as they are defined on the same model geometry. Transverse stress distributions were evaluated at the point of maximum transverse shear force (point S in Fig. 9). Using the output of the FE-analyser $(T; T_{,\alpha}; T_{,\alpha\beta}; \underline{R}; \underline{R}_{,\alpha})$ the independent postprocessor TRAVEST provided the distributions given in Figs. 11 and 12.

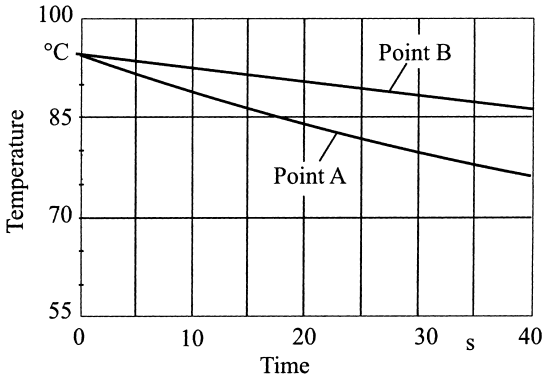

Fig. 10. Cooling curves of top and bottom surface.

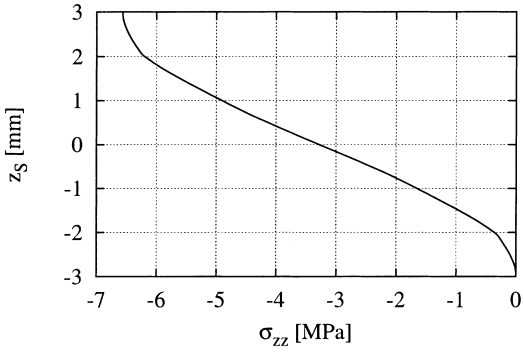

Fig. 11. Transverse normal stress at point S.

4. Conclusions and outlook

The current analysis process for thermo-mechanically loaded composite structures has been demonstrated by the example of two benchmark structures. It turned out to be very costly since different analysis models are needed and the temperature transference involves manual user interaction. A novel high performance finite element analysis process using one shell model throughout has proven to be a big step forward. The modelling as well as the analysis time was

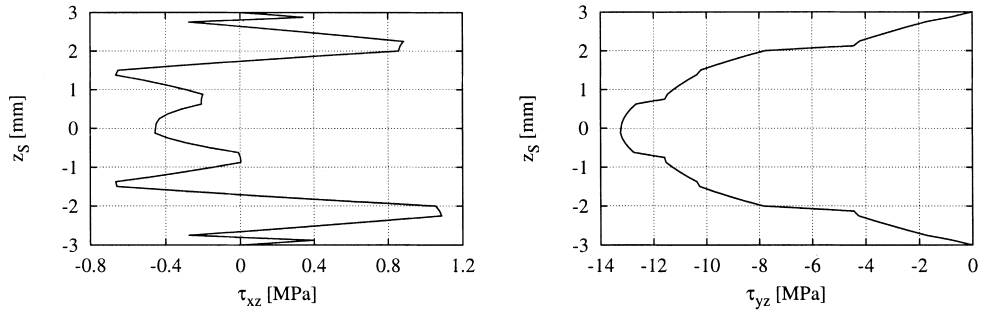

Fig. 12. Transverse shear stresses at point S.

drastically reduced. Within the thermal analysis all kinds of non-linearities including radiation heat transfer could be handled by the finite elements QUADTL and QUADQL. The stress analysis provided not only the in-plane stresses but all transverse stress components as well. Thus, advanced failure criteria for composites accounting for the full state of stress can be applied. Future work should be devoted to hybrid structures consisting of layers from different materials, e.g., sandwich structures, hot structures or thermal protection systems.

Acknowledgements

The analytical 3D-solutions in chapter 3.2 were provided by A.K. Noor (Center or Advanced Computational Technology, Hampton, VA). Intensive discussions of the first author with A.K. Noor led to a deeper understanding of the thermal stress calculation. This is gratefully acknowledged. The analysis of the multiwall-TPS was carried out by our dear colleagues A. de Boer and J.F. Heemskerk from NLR.

References

[1] Argyris J, Tenek L, Öberg F. A multilayer composite triangular element for steady-state conduction/convection/radiation heat transfer in complex shells. Computer Methods in Applied Mechanics and Engineering 1995;120:271–301.

[2] Argyris J, Tenek L. Steady-state nonlinear heat transfer in stiffened composite plates and shells by an exactly integrated facet triangular element. Computer Methods in Applied Mechanics and Engineering 1996;129:53–79.

[3] Block J, Frövel M, Klein H, Petersen D, Rolfes R, Schmidt K, Twardy H. Investigations on thermally resistant structures for future aerospace vehicles. In: AIAA/DGLR Fifth International Aerospace Planes and Hypersonics Technologies Conference, AIAA-93-5086, 1993.

[4] Bose A, Surana KS. Piecewise hierarchical p-version axisymmetric shell element for non-linear heat conduction in laminated composites. Computers and Structures 1993;47:1–18.

[5] Chaudhuri RA. An equilibrium method for prediction of transverse shear stresses in a thick laminated plate. Computers and Structures 1986;23:139–46.

[6] Chin JH, Panczak TD, Fried L. Development of thermal modeling techniques for spacecraft. In: Lewis RW, Chin JH, Homsy GM., editors. Numerical Methods in Thermal Problems. 1991;VII:1315–1325.

[7] Cuntze RG. Effective dimensioning of 3D-stressed UD-laminae on basis of fracture-type strength criteria. In: International Conference on Mechanics of Composite Materials, Riga, 1998.

[8] Dierks A, Rolfes R. Berücksichtigung von Strahlungsrandbedingungen bei der Thermalanalyse von Faserverbundstrukturen mit Hilfe der Methode der finiten Elemente. DLR Report IB131-96/31, Braunschweig, 1996.

[9] Engblom JJ, Ochoa OO. Through-the-thickness stress predictions for laminated plates of advanced composite materials. International Journal for Numerical Methods in Engineering 1985;21:1759–76.

[10] Grallert H, Vollmer K. Conceptual Design of the Thermal Protection System for SÄNGER by Means of Advanced Methods, AIAA-93-5085, 1993.

[11] Hashin Z. Failure criteria for unidirectional fiber composites. Journal of Applied Mechanics 1980;47:329–34.

[12] Heitmeier F, Lederer R, Herrmann O. German Hypersonic Technology Programme-Airbreathing Propulsion Activities, AIAA-92-5057, 1992.

[13] Krammer P, Heitmeier F, Bissinger N, Voss N. German Hypersonics Technology Programme Propulsion Technology-Status 1993, AIAA-93-5094, 1992.

[14] Kwon YW, Akin JE. Analysis of layered composite plates using high-order deformation theory. Computers and Structures 1987;27:619–23.

[15] Murthy, MVV. An improved transverse shear deformation theory for laminated anisotropic plates. NASA Technical Paper 1903, 1981.

[16] Noor AK, Burton WS. Steady-state heat conduction in multilayered composite plates and shells. Computers and Structures 1991;39:185–93.

[17] Padovan J. Steady conduction of heat in linear and nonlinear fully anisotropic media by finite elements. Journal of Heat Transfer 1974;96:313–8.

[18] Pandya BN, Kant T. Flexural analysis of laminated composites using refined higher-order C^0 plate bending elements. Computer Methods in Applied Mechanics and Engineering 1988;66:173–98.

[19] Pryor CW, Barker RM. A finite element analysis including transverse shear effects for application to laminated plates. AIAA Journal 1971;9:912–7.

[20] Puck A. Festigkeitsanalyse von Faser-Matrix-Laminaten, Modelle für die Praxis. München, Wien: Carl Hanser Verlag, 1971.

[21] Reddy JN. A simple higher-order theory for laminated composite plates. Journal of Applied Mechanics 1984;51:745–52.

[22] Reddy JN. A generalization of two-dimensional theories of laminated composite plates. Communications in Applied Numerical Methods 1987;3:173–80.

[23] Rohwer K. Improved Transverse Shear Stiffnesses for Layered Finite Elements. DFVLR-FB 88-32, Braunschweig, 1988.
[24] Rohwer K. Application of higher order theories to the bending analysis of layered composite plates. International Journal Solids and Structures 1992;29:105–19.
[25] Rolfes R. Efficient thermal analysis of anisotropic composite plates using new finite elements. In: Füller J, Grüninger G, Schulte K, Bunsell AR, Massiah A., editors. Developments in the Science and Technology of Composite Materials. Proceedings of the Fourth European Conference on Composite Materials (ECCM4). 1990:743–748.
[26] Rolfes R. Higher order theory and finite element for heat conduction in composites. In: Lewis RW, Chin JH, Homsy GM., editors. Numerical Methods in Thermal Problems, Proceedings of the Seventh International Conference. 1991;7:880–889.
[27] Rolfes R. Nonlinear transient thermal analysis of composite structures. In: Hirsch Ch, Zienkiewicz OC, Onate E., editors. Numerical Methods in Engineering '92, Proceedings of the First European Conference on Numerical Methods in Engineering. 1992:653–659.
[28] Rolfes R, Rohwer K. Improved transverse shear stresses in composite finite elements based on first order shear deformation theory. International Journal for Numerical Methods in Engineering 1997;40:51–60.
[29] Rolfes R, Noor AK, Sparr H. Accurate evaluation of transverse thermal stresses in composite plates based on first-order shear deformation theory. In: Kwon YW, Davis DC, Chung HH, Librescu L. editors. Recent Advances in Solids/Structures and Application of Metallic Materials. ASME International Mechanical Engineering Congress PVP. 1997;369:167–184.
[30] Rolfes R, Noack J, Petersen D, de Boer A, Heemskerk JF, Pauw A. FESTIP-Technology Developments in Heat Management for Reusable Launch Vehicles, Hybrid Structure Analysis Methods. ESA, FTH-DLR-FIR-4000-0002, 1997.
[31] Rolfes R, Rohwer K, Ballerstaedt M. Efficient linear transverse normal stress analysis of layered composite plates.Computers and Structures 1998, accepted for publication.
[32] di M. Bending, vibration and buckling of simply supported thick multilayered orthotropic plates: an evaluation of a new displacement model. Journal of Sound and Vibration 1986;105:425–42.
[33] Senthilnathan NR, Lim SP, Lee KH, Chow ST. Buckling of shear-deformable plates. AIAA Journal 1987;25:1268–71.
[34] Surana KS, Orth NJ. Completely hierarchical axisymmetric shell element based on p-version for heat conduction in laminated composites. Computers and Structures 1981;38:429–48.
[35] Szabo BA, Actis RL. Hierarchic models for laminated plates. In: Adaptive Multilevel and Hierarchical Computational Strategies. AMD-157, 1992:69–94.
[36] Tamma KK, Yurko AA. Unified finite element modelling/analysis approach for thermal-structural response in layered composites. Computers and Structures 1988;29:743–54.